



The influence of carbonate precipitation on riverine magnesium isotope signals: New constrains from Jinsha River Basin, Southeast Tibetan Plateau

Tong Zhao^{a,b,c}, Wenjing Liu^{a,b,c,*}, Zhifang Xu^{a,b,c,*}, Huiguo Sun^{a,b,c},
Xiaode Zhou^{a,b,c}, Li Zhou^d, Jiangyi Zhang^{a,b}, Xuan Zhang^{a,b,c}, Hao Jiang^{a,b,c},
Taoze Liu^e

^a Key Laboratory of Cenozoic Geology and Environment, Institute of Geology and Geophysics, Chinese Academy of Sciences, Beijing 100029, China

^b CAS Center for Excellence in Life and Paleoenvironment, Beijing 100044, China

^c University of Chinese Academy of Sciences, Beijing 100049, China

^d State Key Laboratory of Biogeology and Environmental Geology, China University of Geosciences, Wuhan 430074, China

^e State Key Laboratory of Environmental Geochemistry, Institute of Geochemistry, Chinese Academy of Sciences, Guiyang, Guizhou 550002, China

Received 6 April 2018; accepted in revised form 3 January 2019; available online 11 January 2019

Abstract

Magnesium isotope behavior in dissolution and precipitation reactions during chemical weathering have been well documented. However, mechanisms of mineral dissolution and precipitation impact on the riverine Mg isotope composition under different climatic and geology background are not well constrained, which limits Mg isotope application in weathering research. Mg isotopic compositions for solute and suspended sediments in Jinsha River Basin, located in Tibetan Plateau, China, were examined to address this issue. The $\delta^{26}\text{Mg}$ values for dissolved loads range from -1.67‰ to -0.5‰ , and the suspended loads show systematically heavier Mg isotope compositions (-1.15‰ to -0.06‰). Conservative mixing between different rock weathering end-members fails to fully explain Mg isotopic composition variation of Jinsha River waters based on mass balance and mixing model with the river geochemistry data. Mg in rivers draining dominantly carbonate and evaporite is isotopically heavier compared with the value of catchment bedrocks, and water pH and $\delta^{26}\text{Mg}$ values are negatively correlated in carbonate (calcite and dolomite) oversaturated river waters, which suggests the precipitation of secondary carbonate as an important mechanism driving the $\delta^{26}\text{Mg}$ of dissolved loads heavier. For carbonate unsaturated waters, Mg concentrations and $\delta^{26}\text{Mg}$ values are intermediate between those of silicate dominated basins and carbonate oversaturated waters. The results suggest two possible different mechanisms controlling river solute $\delta^{26}\text{Mg}$ values: fractionation during carbonate precipitation incorporating of Mg; and conservative mixing between a solute end-member formed from carbonate precipitation and end-members from rock weathering. This study provides new evidence and insights in carbonate precipitation processes regulating river Mg isotope signature and its potential influence on Mg cycling.

© 2019 Elsevier Ltd. All rights reserved.

Keywords: River geochemistry; Chemical weathering; Mg isotopes; Secondary carbonate precipitation

* Corresponding authors at: No. 19, Beitucheng Western Road, Chaoyang District, Beijing, China.
E-mail addresses: liuwenjing@mail.iggcas.ac.cn (W. Liu), zfxu@mail.iggcas.ac.cn (Z. Xu).

1. INTRODUCTION

Weathering of Ca-Mg silicate rocks consumes atmospheric CO₂ and regulates global climate over geological timescales. Magnesium is released from primary minerals during weathering reactions, delivered into the oceans via surface and groundwater systems, and is removed from ocean by hydrothermal exchange, marine carbonate deposition and ion exchange reactions with clays (Elderfield and Schultz, 1996). The Mg behavior in chemical weathering is an important process in Mg biogeochemical cycling, and Mg isotope system is applicable of exploring this process. Mg isotopes show limited fractionation during crustal differentiation while large fractionation during chemical weathering (Li et al., 2010). Due to the large relative mass differences (~8% between ²⁴Mg and ²⁶Mg), Mg isotopes are subjected to mass fractionation during weathering reaction and secondary mineral formation, which makes them potential tracers for weathering processes (Pogge von Strandmann et al., 2008; Wimpenny et al., 2011; Opfergelt et al., 2012).

Rivers integrate the weathering and erosion information and material in the basins. Previous studies have suggested lithology as a dominant control on river water chemistry (e.g. Gaillardet et al., 1999). The major source of riverine Mg is carbonate and silicate weathering, which have contrasted Mg isotopic composition values ($\delta^{26}\text{Mg}$), ranging from -5.14‰ to -1.1‰ (Galy et al., 2002; Higgins and Schrag, 2010, 2012, 2015) and -0.7‰ to $+0.9\text{‰}$ (Li et al., 2010; Telus et al., 2012) respectively. Conservative mixing of water mass from different rock weathering end-members has been advocated as the dominant control on Mg isotope composition of river water in many studies (Jacobson et al., 2010; Lee et al., 2014; Fan et al., 2016). However, studies of the mono-lithological silicate catchments have suggested that $\delta^{26}\text{Mg}$ of river waters could not be fully explained by the conservative mixing between different isotopic signatures of drainage bedrocks (e.g. Tipper et al., 2006a). Besides the distinct Mg isotopic composition range of carbonate and silicate rocks, Mg isotopes are well documented of their fractionation during the dissolution and precipitation reactions (Mavromatis et al., 2013; Wimpenny et al., 2014). Dominant control of secondary mineral formation on $\delta^{26}\text{Mg}$ of river water is proposed (Tipper et al., 2006a, 2012; Pogge von Strandmann et al., 2008). Precipitation of secondary phases, which is controlled by the average Mg-O distance in secondary phases, either enriching light Mg in secondary carbonate (Buhl et al., 2007; Galy et al., 2002) or generally favoring heavy Mg in clay minerals (Brenot et al., 2008; Opfergelt et al., 2012; Wimpenny et al., 2014), together with processes such as ion exchange (Jacobson et al., 2010), and plant uptake (Black et al., 2008; Bolou-Bi et al., 2010), are reported as potential factors drifting the river $\delta^{26}\text{Mg}$ away from the value of basin bedrocks. However, how precipitation of secondary minerals influences $\delta^{26}\text{Mg}$ values at basin/global scale, and what is the first order control on the dissolved Mg isotope compositions in river systems with different background remain unclear. Studies about climatic control on riverine Mg isotope composition are rare. Tipper et al.

(2006b) reported different $\delta^{26}\text{Mg}$ values of river water in arctic and tropical environments, but the river Mg isotope variation and its mechanisms in arid regions have not been reported yet. Hence, more explorations on riverine Mg isotopes in different climatic and geologic background settings are worthwhile.

In this study, Jinsha River Basin is selected to explore the behavior of Mg isotopes during weathering processes. As one of the largest rivers draining Tibetan Plateau, Jinsha River is the upper reach of Yangtze River which is the largest river in term of Mg flux to the oceans (approximately equal to Amazon River, Tipper et al., 2006b). The upper-middle reaches of Jinsha River Basin are in arid to semi-arid climate, widely distributed by carbonates and evaporites, and characterized by intense evaporation and carbonate precipitation (e.g. Yang et al., 2015). The river chemistry shows that waters are basically oversaturated with respect to calcite and dolomite in this area (calculated from Wu et al., 2008; Noh et al., 2009). Mg isotopic compositions for both dissolved and suspended loads in the Jinsha River main channel and its tributaries were investigated. We found that the formation of secondary carbonate is an important mechanism driving the Mg isotope composition heavier than conservative mixing process only in Jinsha River waters, and Mg isotopes could be a powerful tool to constrain these processes occurring at basin scale.

2. STUDY AREA

The Jinsha River, the headwater of Yangtze River, is located in the Tibetan Plateau and North Yunnan Plateau. It accounts for approximately 35% of the total river length and 14% of the draining area of Yangtze River which is one of the world's largest river (Noh et al., 2009). The Jinsha River originates from the Geladandong Peak (with an elevation of 6621 m) of the Tanggula Mountains in the north Tibetan Plateau. There are three source tributaries, which are Dangqu River (south source), Chumaer River (north source) and Tuotuo River (the main source). They converge as Tongtian River, which is the upper reaches of Jinsha River, flowing through the Hengduan Mountains and into the warm and humid Sichuan Basin (Fig. 1).

Climate condition shows large spatially and temporally variation in the study area. The mean annual precipitation (MAP) decreases from the southeast to northwest, with 90% precipitation happens during May to October. The evaporation is intense especially in upper reaches of Jinsha River Basin. The Tuotuo River Basin, Chumaer River Basin and Dangqu River Basin in source areas are in cold and dry climate regime, with the mean annual temperature (MAT) below 4 °C, the MAP ranging from 200 mm to 500 mm, and annual evaporation of 1690 mm. Southern areas of this basin (downstream of Jinsha River) are controlled by maritime southwest monsoon and southeast monsoon, which results in a damp and rainy climate there. The MAP in the downstream area of Jinsha River, from Lijiang to Panzhihua, is 900–1300 mm (Wu et al., 2008). Overall, there are three vegetation community types in Jinsha River Basin: the alpine meadow in the source area,

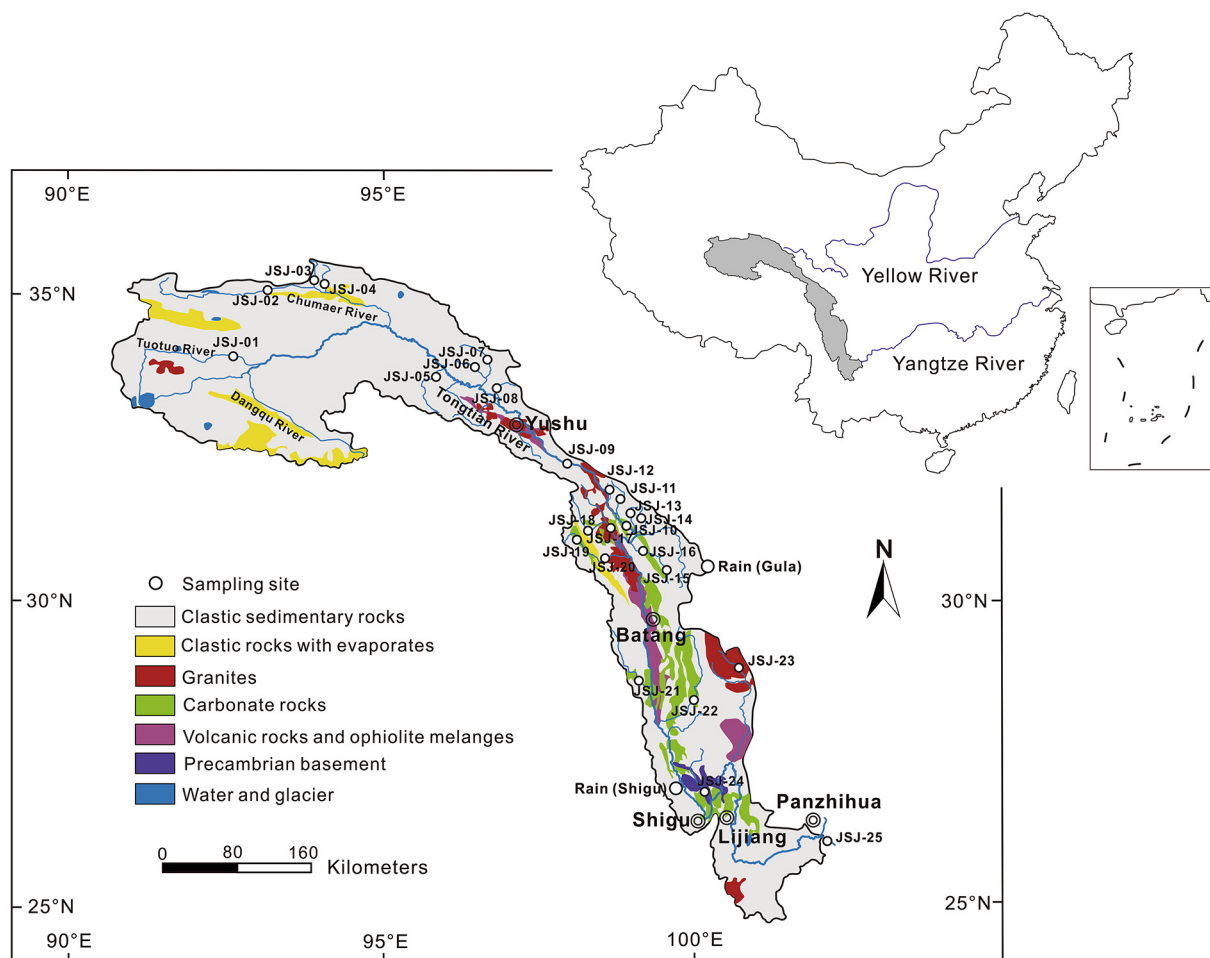


Fig. 1. Map showing sample locations and geology of the Jinsha River Basin, Southeast Tibetan Plateau.

arid-semiarid scrub in the upper-middle reaches (upward from Shigu), and combination of coniferous forest and subtropical forest at the lower reaches (Ren et al., 2016), in accordance with climate regime change. The Jinsha River Basin is relatively pristine, and the average population density of Yushu City is less than 2 persons/km² (website of Ministry of Civil Affairs of the People's Republic of China, available at <http://202.108.98.30>). Anthropogenic input in this basin is negligible (Wu et al., 2008; Noh et al., 2009).

The majority of areas of the Jinsha River Basin are covered by Triassic sedimentary formation, which can be divided into three sedimentary lithologies: clastic rocks (mainly sandstone and slate), limestone occasionally intercalated with volcanic rocks and gypsum beds, and intermediate-acidic volcanic rocks in Upper Triassic; clastic rocks and limestone with volcanic rocks in Middle Triassic; and limestone, sandstone and slate intercalated with basalt and siliceous rocks in Lower Triassic (Editorial Committee of Geology of Three River, 1986). According to the lithology classification (Dürr et al., 2005) and distribution statistics of Jinsha River Basin (Noh et al., 2009), about 70% of the Jinsha River Basin is underlain by mixed consolidated rocks (with 30–70% carbonate), 10% of complex lithology including sedimentary rocks and volcanic rocks with meta-

morphic rocks, and 10% of siliciclastic consolidated rocks mainly consisting of clay, siltstone, mudstone and carbonate. Spatially, the upstream of Jinsha River Basin is covered by clastic rocks with evaporates layers, and rare igneous outcrops. In the river basin downwards from Yushu to Batang, clastic rock, carbonate and granitoid rocks are widely distributed. Some ophiolitic melanges were found at the suture zones near Batang, dominated by basic and ultrabasic rock and limestone (Wang et al., 2000). Precambrian high grade metamorphic rocks expose around Shigu, the first big bend of the Yangtze River. Clastic rocks, carbonates, fluvial deposits and granites are distributed throughout the lower reaches from Shigu to Panzhuhua.

3. FIELD AND ANALYTICAL TECHNIQUES

3.1. Sampling

River waters and suspended sediments were collected along the Jinsha River in July, 2013. Temperature, pH and electrical conductivity were measured in the field with a portable EC/pH meter (pH/°C: ±0.05/0.5 °C). Water samples were filtered in the field through 0.22 μm cellulose acetate filters, and the alkalinity was titrated by hydrochloro-

ric acid in the same day of sampling. Filtered water samples were stored in pre-acid-cleaned high density polyethylene bottles and those for analysis of cations and Mg isotopes were acidified to $\text{pH} < 2$ with ultrapure HNO_3 . Two rain samples were collected at Shigu and Gula village respectively (Fig. 1).

3.2. Analytical methods

Suspended sediments were grounded to 200 mesh and dissolved in high pressure bomb using a mixture of concentrated HNO_3 -HF (1:1, v/v) in 190 for 48 h and dried up with 1 ml HNO_3 twice, and finally dissolved in 2% HNO_3 for chemistry analyzing and in 1 N HNO_3 for Mg separation. Concentrations of cations and anions for the water samples were determined using Perkin Elmer inductively coupled plasma mass spectrometry (model Elan DRC-e) and Dionex Ion Chromatography (model ICS-1500) with uncertainties better than 5% and 10%, respectively. The mineral compositions of suspended sediment were determined by X-ray Diffraction (XRD) (Bruker D8 Advance) with a scan speed of 1° min^{-1} . The chemical purification procedure of Mg employed in this study was adapted from Teng et al. (2007). The chromatographic purification was processed in a Saville micro-column filled with 2 ml Bio-Rad AG50-X12 (200–400 mesh) cation resin. The resin was conditioned with 5 ml 1 N HNO_3 and then sample with 20 μg Mg was loaded and eluted by 1 N HNO_3 . Since Mg isotopes can be significantly fractionated during ion exchange processes, it is obligatory to obtain Mg yield close to 100%. The total blank and the recovery of the sample purification procedure were $< 10 \text{ ng}$ and $> 99\%$, respectively. Chemistry analysis and Mg purification were conducted in the hydrochemistry and environmental laboratory at the Institute of Geology and Geophysics, Chinese Academy of Sciences.

Mg isotope ratios were measured by Neptune Plus MC-ICP-MS at the Isotope Geochemistry Laboratory of the China University of Geosciences, Beijing. The Mg concentration of the sample was adjusted to the same concentration ($\pm 10\%$) as the standard, about 400 ppb, which yields beam intensity of $\sim 8 \text{ V}$ for ^{24}Mg with background Mg signals $< 10^{-4} \text{ V}$. All samples and standards were introduced to the Ar plasma in 3% HNO_3 using a “wet” sample introduction system with a quartz spray chamber and a 50 $\mu\text{l}/\text{min}$ PFA nebulizer. A single analysis of Mg isotope ratio is corresponded to one bracket using standard-sample bracketing method (DSM-3 as standard), the standard-sample sequence was repeated 4 times for each sample to get a reproducibility. All data are reported in delta notation relative to DSM-3:

$$\delta^x \text{Mg} = \left(\frac{\left(\frac{{}^x \text{Mg}/{}^{24} \text{Mg}}{\left(\frac{{}^x \text{Mg}/{}^{24} \text{Mg}}{\text{DSM-3}} \right)} \right)_{\text{sample}}}{\left(\frac{{}^x \text{Mg}/{}^{24} \text{Mg}}{\text{DSM-3}} \right)} - 1 \right) \times 1000 \quad (1)$$

where $x = 25$ or 26 . Long term external precision (2SD) is $\pm 0.06\text{‰}$ for $\delta^{26}\text{Mg}$ and $\pm 0.05\text{‰}$ for $\delta^{25}\text{Mg}$ (Ke et al., 2016). Reduplicated measurements of the BHVO-2 yield average $\delta^{26}\text{Mg} = -0.23\text{‰} \pm 0.02$ (2SD, $n = 10$), identical

to those reported in the previous studies within uncertainty (Huang et al., 2012; Ke et al., 2016). The instrument working condition was detailed in Ke et al. (2016).

4. RESULTS

4.1. Major element concentrations

The electrical conductivities of river water show large variations, ranging from 21 to 2387 $\mu\text{S}/\text{cm}$. Concentrations of dissolved elements vary significantly, from 41.1 to 1471.9 $\mu\text{mol}/\text{L}$ for Mg, 38.5 to 1942.3 $\mu\text{mol}/\text{L}$ for Ca, 51.9 to 15025.4 $\mu\text{mol}/\text{L}$ for Na. Calcite saturation index (CSI) and dolomite saturation index (DSI) were calculated (Table 1) with PHREEQC program (Parkhurst and Appelo, 1999) to evaluate the calcite and dolomite saturation status for river waters. River waters which are calcite oversaturated are generally dolomite oversaturated.

The head water of the Jinsha River shows significant evaporite influence on water chemistry, which is in accordance with previous studies (e.g. Wu et al., 2008; Noh et al., 2009). Two headwater tributaries (JSJ-01 and JSJ-02) exhibit extremely high Na^+ , Ca^{2+} , Cl^- , and SO_4^{2-} concentrations, which are supposed to be the result of halite and gypsum/anhydrite dissolution. These ion concentrations generally decrease along mainstreams resulted by dilution effect (Table 1). Significant correlations are observed between Na^+ and Cl^- ($R^2 = 0.99$), K^+ and Cl^- ($R^2 = 0.84$, except JSJ-02), and SO_4^{2-} is positively correlated with Ca^{2+} ($R^2 = 0.53$). Gypsum/anhydrite is scattered throughout the upper basin area, and the importance of Mg-associated SO_4^{2-} in river water is emphasized (Noh et al., 2009). The saline lakes (e.g. Hoh Xil Lake, Zhuonai Lake, and Xijir Ulan Lake) located in the vicinity of source area of Jinsha River Basin are mainly magnesium sulfate subtype lakes with high Mg^{2+} and SO_4^{2-} concentrations (Zheng and Liu, 2010). The associated mineral assemblages of these lakes are epsomite, bloedite, and bischofite. An excess of SO_4^{2-} relative to Ca^{2+} concentration was observed for sample JSJ-02, showing the possible existence of magnesium or sodium sulfate salts. Ca^{2+} and HCO_3^- are the dominant ions in river waters, and HCO_3^- is well-correlated with Ca^{2+} ($R^2 = 0.94$), implying significant solute contribution from carbonate weathering in Jinsha River waters.

4.2. Magnesium isotopic compositions

Dissolved loads show a wide range of $\delta^{26}\text{Mg}$ values (from -1.67‰ to -0.50‰), within the ranges of dissolved loads from world other watersheds, e.g. Yellow River (-1.53‰ to -0.11‰ , Fan et al., 2016), Marsyandi River at south Himalaya (-2.08‰ to -0.77‰ , Tipper et al., 2008), and Mackenzie River (-1.7‰ to -0.86‰ , Tipper et al., 2012). The main channel is characterized by a narrow solute $\delta^{26}\text{Mg}$ range from -1.25‰ to -0.86‰ . Water samples are characterized by systematically lighter Mg isotope composition relative to the suspended loads, which range from -1.15‰ to -0.06‰ (Table 2). Two rain waters with similar $\delta^{26}\text{Mg}$ values at -1.84‰ and -1.82‰ , are isotopically lighter than the river waters, seawater (-0.82‰ ,

Table 1
Elemental concentrations and Mg isotopic compositions of river water.

Samples	pH	T	HCO ₃ ⁻ μmol/L	F ⁻ μmol/L	Cl ⁻ μmol/L	NO ₃ ⁻ μmol/L	SO ₄ ²⁻ μmol/L	SiO ₂ μmol/L	K μmol/L	Na μmol/L	Ca μmol/L	Mg μmol/L	δ ²⁵ Mg ‰	2σ	δ ²⁶ Mg ‰	2σ	CSI	DSI
<i>Tributaries</i>																		
JSJ-01	7.87	13.7	2484.9	12.5	5841.6	3.9	748.0	115.2	286.9	6050.6	1107.1	455.2	-0.49	0.02	-0.96	0.04	0.01	-0.39
JSJ-03	7.86	12.9	1570.7	6.9	858.5	8.2	202.7	39.4	57.0	758.9	579.2	380.1	-0.53	0.01	-0.99	0.06	-0.39	-1.00
JSJ-04	7.89	15.4	2436.3	6.4	2774.4	11.1	853.7	54.4	48.1	2260.4	892.8	1257.5	-0.38	0.03	-0.74	0.06	-0.03	0.09
JSJ-05	8.27	17.8	2466.1	5.0	232.7	105.9	347.5	61.6	26.2	466.5	1207.0	420.1	-0.63	0.05	-1.25	0.02	0.58	0.73
JSJ-06	8.28	15.3	3289.7	6.3	61.9	98.6	83.0	115.2	29.5	250.6	1407.6	454.8	-0.62	0.05	-1.22	0.03	0.74	1.00
JSJ-07	8.13	15.3	3585.5	3.7	242.6	164.6	1086.5	84.5	25.3	472.2	1495.1	1471.9	-0.29	0.01	-0.59	0.03	0.59	1.17
JSJ-08	8.15	10.3	4070.7	9.0	397.7	116.8	1037.6	99.5	38.2	1006.9	1779.9	1109.2	-0.37	0.05	-0.75	0.03	0.66	1.03
JSJ-11	7.05	11.6	2295.7	11.6	16.5	96.7	194.3	78.8	32.6	101.4	939.1	464.1	-0.51	0.01	-0.99	0.05	-0.92	-2.22
JSJ-12	7.55	12.2	1751.3	3.1	12.5	51.1	284.4	82.3	19.1	57.1	976.4	253.9	-0.49	0.03	-0.98	0.05	-0.45	-1.54
JSJ-13	6.92	13.2	2035.3	3.2	13.0	85.1	197.8	88.1	24.9	66.9	911.1	387.2	-0.54	0.04	-1.06	0.05	-1.11	-2.63
JSJ-14	7.87	15.7	1285.1	16.9	12.4	87.0	89.4	80.9	20.0	78.9	539.7	219.0	-0.56	0.04	-1.07	0.03	-0.42	-1.23
JSJ-15	8.00	14.0	1396.3	5.7	10.7	59.4	175.0	78.8	20.2	81.7	653.4	243.4	-0.42	0.02	-0.83	0.01	-0.21	-0.87
JSJ-16	7.93	14.7	1396.3	3.0	9.8	61.8	541.9	91.6	10.5	73.1	762.9	514.2	-0.26	0.03	-0.5	0.02	-0.24	-0.66
JSJ-17	8.32	14.7	2596.2	5.0	30.8	104.9	141.2	108.1	19.4	141.2	1186.2	236.2	-0.71	0.05	-1.37	0.03	0.62	0.52
JSJ-18	8.21	14.7	1928.8	4.2	13.9	117.1	150.2	116.0	15.6	116.2	915.6	170.8	-0.65	0.03	-1.26	0.04	0.29	-0.17
JSJ-19	8.22	14.3	2189.2	4.8	35.0	124.4	238.6	98.1	25.7	254.1	917.6	293.4	-0.66	0.04	-1.23	0.05	0.33	0.15
JSJ-20	8.31	15.2	2769	6.5	62.5	100.3	149.2	120.2	27.5	290.0	1212.7	351.7	-0.61	0.03	-1.22	0.06	0.64	0.75
JSJ-21	8.38	16.0	2352.7	4.6	46.9	1.2	51.1	90.9	35.6	146.9	850.9	243.1	-0.86	0.02	-1.67	0.05	0.53	0.52
JSJ-22	8.21	13.1	757.1	2.7	9.5	11.9	25.3	125.3	11.8	91.8	262.1	78.2	-0.48	0.05	-0.93	0.04	-0.62	-1.80
JSJ-23	7.69	14.0	316.4	1.7	4.6	7.8	5.4	84.5	9.7	58.5	84.7	41.1	-0.59	0.03	-1.14	0.04	-1.97	-4.30
JSJ-24	7.16	17.9	839.6	2.0	17.2	15.0	15.7	116.7	23.2	71.1	304.2	85.7	-0.61	0.03	-1.22	0.03	-1.54	-3.60
<i>Mainstreams</i>																		
JSJ-02	7.72	14.0	1878.1	15.7	15044.3	4.6	2438.3	58.7	139.0	15030.6	1988.5	916.5	-0.65	0.03	-1.25	0.06	-0.11	-0.59
JSJ-09	8.15	15.4	2840	9.3	3368.0	132.9	810.6	95.2	92.8	3750.4	1371.3	814.0	-0.44	0.03	-0.86	0.02	0.47	0.72
JSJ-10	8.20	15.7	2816.3	9.0	2552.5	138.4	756.9	98.8	76.1	2838.0	1301.2	764.2	-0.49	0.05	-1.01	0.03	0.51	0.80
JSJ-25	7.27	22.2	2171.9	7.8	1458.3	6.5	425.4	100.9	52.5	1599.4	885.8	446.7	-0.56	0.04	-1.07	0.03	-0.58	-1.37
<i>Rain</i>																		
Shigu				0.0	19.1	13.8	16.1		8.5	25.1	184.3	30.4	-0.95	0.04	-1.84	0.04		
Gula				0.9	7.9	6.9	10.4		3.8	7.7	83.4	13.9	-0.95	0.02	-1.82	0.06		

Table 2
Elemental concentrations and Mg isotopic compositions of suspended load and epsomite.

Samples	Na	K	Mg	Ca	Rb	$\delta^{25}\text{Mg}$	2σ	$\delta^{26}\text{Mg}$	2σ
	mg/g	mg/g	mg/g	mg/g	$\mu\text{g/g}$	‰			
<i>Tributaries</i>									
JSJ-01	7.21	36.42	12.00	45.90	632.4	-0.14	0.02	-0.28	0.04
JSJ-03	11.61	28.50	12.74	28.67	323.0	-0.20	0.05	-0.40	0.05
JSJ-04	11.46	32.76	11.12	40.64	300.1	-0.20	0.02	-0.41	0.03
JSJ-05	9.68	20.71	16.54	87.28	222.0	-0.60	0.02	-1.15	0.01
JSJ-06	8.39	20.59	8.11	38.34	229.3	-0.17	0.04	-0.34	0.02
JSJ-07	10.20	22.05	8.97	40.27	246.2	-0.22	0.02	-0.45	0.03
JSJ-08	10.83	26.81	12.90	32.80	250.5	-0.20	0.04	-0.44	0.05
JSJ-11	5.04	36.68	10.78	32.96	397.0	-0.10	0.02	-0.23	0.06
JSJ-12	6.72	33.21	12.26	15.51	348.0	-0.07	0.05	-0.16	0.07
JSJ-13	7.09	29.75	10.95	24.97	304.8	-0.13	0.03	-0.28	0.06
JSJ-14	7.43	28.82	13.23	22.88	303.0	-0.15	0.03	-0.27	0.03
JSJ-15	6.58	33.24	13.05	6.77	387.2	-0.11	0.03	-0.19	0.04
JSJ-16	5.88	28.10	19.99	22.76	324.5	-0.02	0.04	-0.08	0.04
JSJ-17	6.81	25.46	10.81	43.70	291.5	-0.08	0.05	-0.17	0.05
JSJ-18	8.99	21.63	8.92	39.64	242.8	-0.11	0.06	-0.19	0.01
JSJ-19	17.72	24.67	17.72	30.34	351.2	-0.16	0.05	-0.33	0.06
JSJ-20	7.00	25.18	10.92	30.74	279.8	-0.11	0.04	-0.21	0.02
JSJ-21	1.68	36.30	14.90	10.37	421.9	-0.06	0.04	-0.10	0.06
JSJ-22	4.84	24.37	14.57	21.44	264.4	-0.47	0.04	-0.89	0.06
JSJ-23	10.61	29.42	11.80	8.10	364.1	-0.14	0.01	-0.28	0.06
JSJ-24	1.51	31.91	6.77	6.00	449.2	-0.01	0.04	-0.06	0.04
<i>Mainstreams</i>									
JSJ-02	6.38	38.88	19.13	45.23	325.6	-0.24	0.03	-0.46	0.04
JSJ-09	6.98	27.96	10.17	66.21	234.3	-0.30	0.01	-0.62	0.05
JSJ-10	7.13	22.65	11.48	78.64	266.3	-0.32	0.04	-0.58	0.04
JSJ-25	6.24	27.57	12.27	46.28	338.1	-0.17	0.05	-0.33	0.03
<i>Epsomite</i>									
						-0.58	0.03	-1.16	0.05
						-0.58	0.02	-1.11	0.04

Young and Galy, 2004) and silicate rocks (-0.7‰ to $+0.9\text{‰}$, Li et al., 2010; Telus et al., 2012). The epsomite samples collected in the source area show $\delta^{26}\text{Mg}$ values of -1.16‰ and -1.11‰ . All samples fall on a line with a slope

of 0.521 in a $\delta^{26}\text{Mg}$ vs. $\delta^{25}\text{Mg}$ diagram (Fig. 2), in consist with the slope of the terrestrial equilibrium mass fractionation line reported by Young and Galy (2004).

5. DISCUSSION

5.1. Correction for atmospheric input

Correcting atmospheric contribution to riverine Mg budgets is the first step when evaluating the influence of weathering on the Mg isotope composition of rivers. It is critical to exclude evaporite and anthropogenic Cl^- during the correction. Collected from a silicate and pristine catchment, sample JSJ-23 has the lowest Cl^- concentration of $4.6 \mu\text{mol/L}$ in all river waters, which is within the Cl concentration of local long-term precipitation ($0.9\text{--}32.7 \mu\text{mol/L}$, Zhang et al., 2012). The Cl^- of river sample JSJ-23 is assumed to be entirely from atmospheric precipitation. The long term average Mg/Cl molar ratio in rain waters is 0.67 (Zhang et al., 2012), thus Mg concentration of rain water is calculated at $3.1 \mu\text{mol/L}$. Then we estimated the proportion of Mg derived from precipitation to Mg in rivers is 0.2–8%. Using a standard isotope mass-balance equation, the corrected riverine $\delta^{26}\text{Mg}$ are lowered by less than 0.05‰ from measured riverine $\delta^{26}\text{Mg}$, within the long term external precision ($\pm 0.06\text{‰}$). The impact of atmospheric precipitation to riverine $\delta^{26}\text{Mg}$ values is negligible.

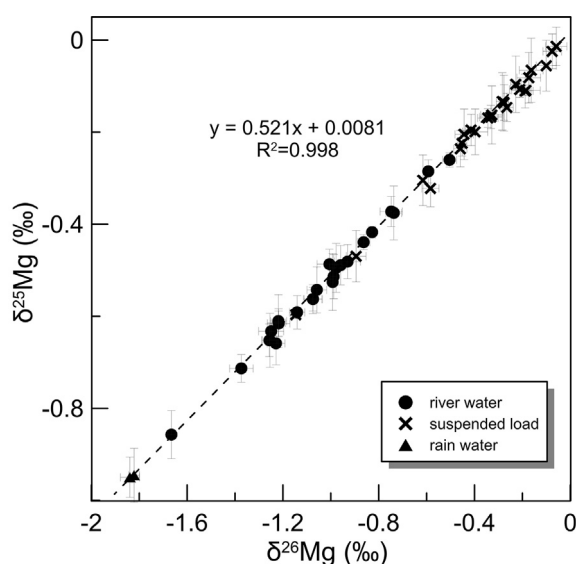


Fig. 2. All samples analyzed in this study fall on a single isotopic mass-dependent fractionation line on the Mg three-isotope diagram.

5.2. Biological control

Both experimental studies (Black et al., 2008; Bolou-Bi et al., 2010) and field observations (Tipper et al., 2010) have demonstrated that Mg isotopes are fractionated during plant uptake. The plants preferentially take heavier Mg isotopes (Black et al., 2008), thus potentially driving $\delta^{26}\text{Mg}$ of solutions lower. However, there is a lack of evidence for plant uptake effect on river water Mg isotopic compositions (Wimpenny et al., 2011; Tipper et al., 2012; Fan et al., 2016), even in a strong vegetation gradient basin (Tipper et al., 2008). Bolou-Bi et al. (2010) estimated that, at the global scale, even if 40% of river dissolved Mg originates from litter degradation, increase of $\delta^{26}\text{Mg}$ values in river waters is still limited ($\sim 0.25\text{‰}$). The sampling sites were generally with elevation over 3000 m and the vegetation (mainly herbage and thorny shrubs) are not well developed (Ren et al., 2016). Based on the previous observation and evaluation, we exclude the effect of plant uptake as the major control of riverine $\delta^{26}\text{Mg}$ in the study basin.

5.3. Lithological control

The Mg isotope compositions of river water are intermediate between silicates and carbonates (Fig. 5a and Table 1). It seems that Mg isotopic composition of river waters is the result of conservative mixing between silicate and carbonate end-members. However, $\delta^{26}\text{Mg}$ values does not correlate with potential index for identifying carbonate and silicate end-members, such as Ca/Si ($R^2 = 0.006$), implying that conservative mixing of silicate and carbonate rock weathering end-member is not the only mechanism controlling river Mg isotope composition.

In river water, Mg derived from silicate weathering (Mg_{sil}) can be estimated by the following equation (Galy and France-Lanord, 1999):

$$\text{Mg}_{\text{sil}} = \text{Na}_{\text{sil}} \times \left(\frac{\text{Mg}}{\text{Na}} \right)_{\text{sil}} \quad (2)$$

In the equation, Na_{sil} is silicate weathering derived Na, and $(\text{Mg}/\text{Na})_{\text{sil}}$ is the molar ratios of silicate weathering end-member. Generally, the $(\text{Mg}/\text{Na})_{\text{sil}}$ ratios can be obtained based on either the dissolved composition of small silicate monolithologic drainages within the study area, or local silicate bedrock chemistry. Previous studies have documented the element ratios (such as Mg/Na) of silicate end-member for river basins in Tibetan Plateau to estimate silicate weathering rate. For example, In adjacent river basins of Jinsha River, the $(\text{Mg}/\text{Na})_{\text{sil}}$ ratio of 0.26 was employed for Min Jiang (Yoon et al., 2008), 0.16 for Red River (Moon et al., 2007), and 0.3 ± 0.2 for Himalaya rivers (Krishnaswami and Singh, 1999). Moreover, the Mg/Na ratio of silicate rocks in small granite catchments in east Tibetan Plateau was reported at 0.25 (Jiang et al., 2018), and the Mg/Na ratios of silicate bedrock data compiled by Wu et al. (2008) in Jinsha River Basin are 0.18–0.43. Here we adopted the $(\text{Mg}/\text{Na})_{\text{sil}}$ value of 0.24 ± 0.12 from Gaillardet et al. (1999), which has also been used by Noh et al. (2009) in their analyses of silicate weathering rate in Jinsha Rivers.

It is calculated that silicate weathering contributes 0–38% of dissolved Mg to river, averaging at $\sim 10\%$. Considering that sodium sulfate exists in source area of the basin (Wu et al., 2008), and the proportion of sodium sulfate (such as $\text{Na}_{\text{mirabilite}}/\text{Na}_{\text{halite}}$) in evaporite is unknown, the calculated Mg_{sil} is an upper limit of silicate Mg. The contemporaneous Triassic granites have the $\delta^{26}\text{Mg}$ between -0.26‰ and -0.14‰ (Liu et al., 2010) and $\delta^{26}\text{Mg}$ value of the basalt in the basin have been reported from -0.45‰ to -0.51‰ (Tian et al., 2018). Thus assuming a silicate rock end-member $\delta^{26}\text{Mg}$ value of -0.2‰ (value of Upper Continental Crust, Li et al., 2010), the simple mass balance model shows that there should be a non-silicate (carbonate or evaporite) end-member with $\delta^{26}\text{Mg}$ value as high as -0.5‰ (the $\pm 50\%$ uncertainty of $(\text{Mg}/\text{Na})_{\text{sil}}$ has little influence ($\pm 0.02\text{‰}$) on the estimated value), which is significantly higher than current accepted carbonate $\delta^{26}\text{Mg}$ range (-5.14‰ to -1.1‰ , Galy et al., 2002; Higgins and Schrag, 2010, 2012, 2015; Jacobson et al., 2010; Pokrovsky et al., 2011; Riechelmann et al., 2012). Another potential contributor for riverine Mg is evaporites. The $\delta^{26}\text{Mg}$ value of gypsum which is the most widely existent evaporite was reported at -0.8‰ (Brenot et al., 2008). The gypsum in Jinsha River Basin have very low Mg content, as well as Mg/Ca ratio (Mg/Ca molar ratio at 1×10^{-4} , Tian et al., 2017). The $\delta^{26}\text{Mg}$ values of epsomite in this basin are about -1.1‰ , which are comparable to $\delta^{26}\text{Mg}$ value of rivers, the water chemistry of which is characterized by evaporite dissolution (JSJ-1 and JSJ-2, $\delta^{26}\text{Mg}$ of -1.25‰ and -0.96‰). So, the estimated $\delta^{26}\text{Mg}$ of non-silicate end-member falls out of any documented evaporite $\delta^{26}\text{Mg}$ range, and the conservative mixing cannot fully explain the magnesium isotope data in Jinsha River Basin. Many studies have argued lithology as the dominant control on Mg isotope compositions in river and groundwater (e.g. Brenot et al., 2008; Jacobson et al., 2010; Fan et al., 2016), while it is questionable in Jinsha River Basin. Further end-members and alternative mechanism investigation for Mg isotope systems are needed.

5.4. Mg isotope fractionation during secondary mineral formation

5.4.1. Clay formation

River suspended sediments represent the solid weathering product, including secondary minerals and residual primary minerals. The mineral composition determines the geochemical signature of suspended sediment, thus the Mg isotope composition. The $\delta^{26}\text{Mg}$ values of suspended load range from -1.15‰ to -0.06‰ , which is slightly lower than the reported $\delta^{26}\text{Mg}$ range of suspended loads in typical silicate-draining rivers (e.g. -0.84‰ to 0.53‰ of basaltic rivers in Iceland, Pogge von Strandmann et al., 2008, and -0.46‰ to -0.27‰ of rivers draining silicate metamorphic rock in West Greenland, Wimpenny et al., 2011). A linear relationship ($R^2 = 0.47$) between the $\delta^{26}\text{Mg}$ value and Ca/Mg ratio was observed for suspended loads (Fig. 3). The relationship reveals a mixture of two Mg end-members, which are primary silicate minerals and clay with high $\delta^{26}\text{Mg}$ value and low Ca/Mg ratio, and carbonate

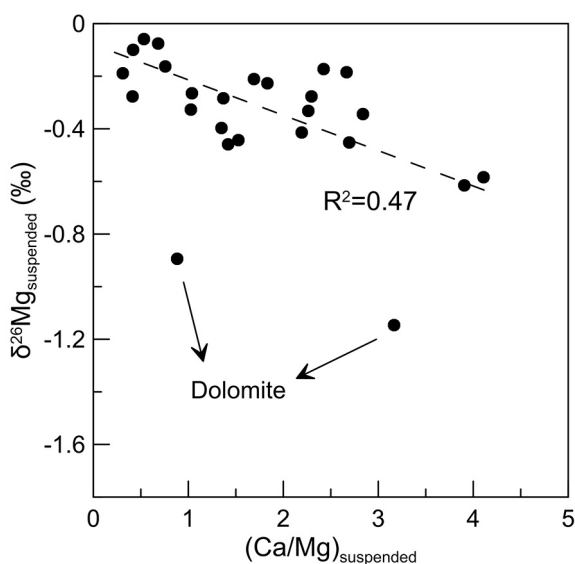


Fig. 3. The relation between Ca/Mg molar ratios and $\delta^{26}\text{Mg}$ values in suspended load.

with low $\delta^{26}\text{Mg}$ and high Ca/Mg ratio. This is assumed to be the reason for the lowered suspended $\delta^{26}\text{Mg}$ range for Jinsha River basin compared with other silicate basins. The suspended loads of JSJ-5 and JSJ-22 are two anomalies in the plot, which have relatively low $\delta^{26}\text{Mg}$ values and fall outside the linear relationship. This was supposed to be the result of detrital dolomite contamination. From this point, the $\delta^{26}\text{Mg}$ value of dolomite in this basin should be lower than -1.15‰ , which is in accordance with the average $\delta^{26}\text{Mg}$ value of documented dolomite ($-1.75 \pm 1.08\text{‰}$, Geske et al., 2015).

The mineral compositions of suspended load were chlorite (mainly chinocllore) and kaolinite as clay minerals, and quartz, albite, muscovite and calcite as non-clay minerals according to XRD analysis (Table S1). Chlorite is the dominated Mg residence clay in the suspended materials in Jinsha River. Previous studies have argued that secondary mineral formation plays an important role in controlling Mg isotopic compositions in river waters (Tipper et al., 2006a; Pogge von Strandmann et al., 2008). However, the influence of clay formation on river $\delta^{26}\text{Mg}$ is very limited in Jinsha River Basin where carbonate weathering contribution dominates the water chemistry (Brenot et al., 2008; Lee et al., 2014; Fan et al., 2016). First, the proportion of Mg in river water from silicate weathering is small (averaging at $\sim 10\%$ of total) compared with those from carbonate and evaporite. Besides, the fractionation factor for chlorite is 1.0005 (Wimpenny et al., 2014), and the formation of chlorite would drive the $\delta^{26}\text{Mg}$ value of river water lower, which cannot explain the inferred non-silicate end-member with isotopically heavy Mg (discussed in Section 5.3).

Rb concentrations in suspended load are employed to indicate clay content in previous studies as it is uniquely hosted in the interlayer crystallographic sites of clays (Tipper et al., 2012). In Jinsha River Basin, based on the available data, the clay content is positively correlated with Rb concentration in suspended load ($R^2 = 0.84$, Fig. S1),

which confirmed the indication of Rb concentration for clay content. The relationship between Rb content and $\delta^{26}\text{Mg}$ values of suspended load are plotted in Fig. 4a, the data is adequately described by a ternary mixture of carbonate with low Rb content and $\delta^{26}\text{Mg}$ value, clay with high Rb content and $\delta^{26}\text{Mg}$, and primary mineral with low Rb content and high $\delta^{26}\text{Mg}$ such as albite, indicating the mineralogy control on Mg isotope composition of suspended load. In contrast with the trend documented by Tipper et al. (2012), no correlations are observed between Rb content of suspended load and water $\delta^{26}\text{Mg}$ (Fig. 4b). The signal of clay fractionation impact on dissolved loads is assumed to be limited and are more likely overprinted by other Mg rich mineral weathering processes, such as carbonate and evaporite dissolution in Jinsha River water.

5.4.2. Carbonate precipitation

The northeast Tibetan Plateau is characterized by arid climate, intense evaporation and widely carbonate precipitations (Yang et al., 2015). Up to 70% of Ca is estimated to be lost from river waters by precipitation of secondary calcite in the arid climate area of the Tibetan Plateau (Jacobson et al., 2002). Based on the discussion above and the basin background, we propose the hypothesis that the carbonate precipitation might regulate the riverine Mg isotope composition in Jinsha River. It has been well documented that light Mg is preferentially incorporated into carbonate during its precipitation by experimental and field studies (e.g. Galy et al., 2002; Mavromatis et al., 2013; Trostle et al., 2014; Zhang et al., 2018). Thus, the formation of secondary carbonate in river basin has the potential to drift the Mg isotope composition of river water heavier.

In Jinsha River Basin, river waters in upper and middle reaches under the arid climate and high alkalinity are basically oversaturated with respect to both calcite and dolomite (Table 1). As shown in Fig. 5a, the presented 1/Mg and $\delta^{26}\text{Mg}$ relationship cannot be explained by mixing model alone, especially the samples with high $\delta^{26}\text{Mg}$ values and low 1/Mg. Although these samples have overlapped $\delta^{26}\text{Mg}$ range with silicate draining rivers (between -0.96‰ and $+0.3\text{‰}$, Tipper et al., 2006b; Pogge von Strandmann et al., 2008), the Mg concentrations is much higher. Evaporation of silicate draining river waters might be a potential mechanism to explain the samples locating outside the mixing zone of the three end-members. The Dousitu River Basin which is located in arid area of northeastern Tibetan Plateau with annual precipitation and evaporation at 267 mm and 2459 mm (~ 10 times difference) respectively, has more intense evaporation effect than Jinsha River Basin. The modeled result for the percentage of evaporated rain volume in Dousitu River is between 10–30% (Qian et al., 2007). As the dominated sources of river water, it is reasonable to say that the condensing effect on ion concentration by evaporation would be limited to less than 30%. Besides, evaporation is 3–7 times higher than precipitation in upper-middle reaches of Jinsha River Basin, which is lower than Dousitu River. So, the enrichments of ion concentration due to evaporation in Jinsha River Basin should be weaker than Dousitu River Basin. However, the Mg concentration is 5–10 times higher than

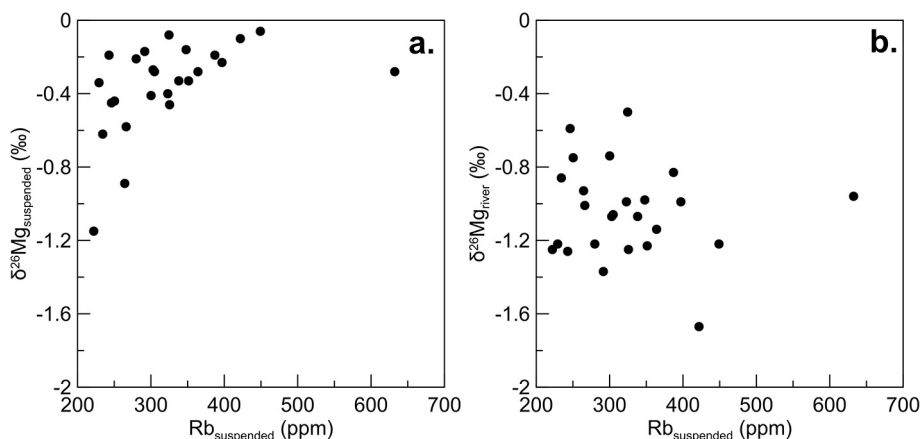


Fig. 4. Rb concentrations of suspended load versus $\delta^{26}\text{Mg}$ values of suspended loads (a) and $\delta^{26}\text{Mg}$ values of river waters (b).

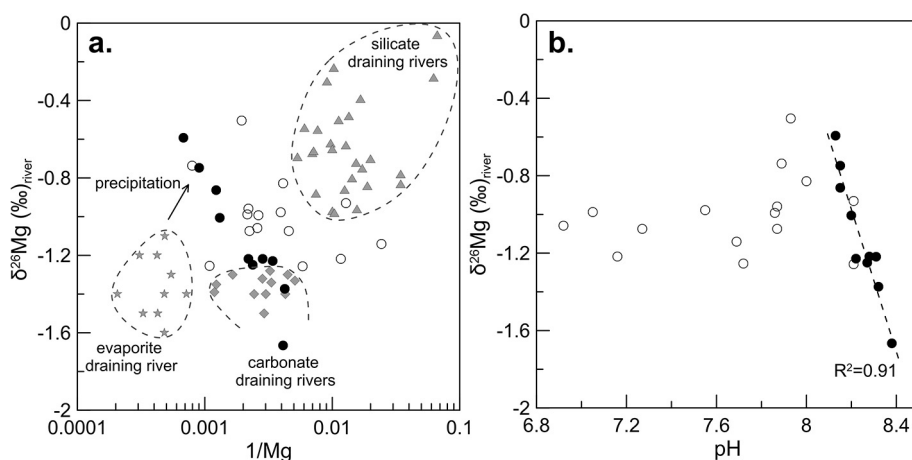


Fig. 5. (a) The relationships between $1/\text{Mg}$ and $\delta^{26}\text{Mg}$ values, and (b) water pH and $\delta^{26}\text{Mg}$ values of river waters. Solid circles correspond to calcite and dolomite oversaturated river waters, and open circles correspond to calcite and dolomite unsaturated river waters. Mg concentration and $\delta^{26}\text{Mg}$ data of rivers draining silicate rocks are from Tipper et al. (2006b), Lee et al. (2014) and Pogge von Strandmann et al. (2008). Data of rivers draining carbonate rocks is from Tipper et al. (2006b), Lee et al. (2014) and Brenot et al. (2008). Data of river draining basins contain evaporite is from Brenot et al. (2008).

the proposed silicate draining river end-members. So, evaporation of silicate draining river waters is excluded as the dominated mechanism for the high Mg concentration in samples outside the mixing zone.

In Fig. 5a and b, carbonate oversaturated and unsaturated river water are separated into two different trending groups, which suggests that carbonate precipitation have modified Mg isotope compositions and Mg concentration in river water. The pH value could be an indicator of carbonate precipitation process. H^+ is released from HCO_3^- during the incorporation of CO_3^{2-} into carbonate phases, which causes the decreasing of pH values (Plummer et al., 1990; Jacobson et al., 2010). The fractionation of Mg isotopes by secondary carbonate precipitation in Jinsha River Basin is well indicated by the strong negative correlation ($R^2 = 0.91$, Fig. 5b) between water pH and $\delta^{26}\text{Mg}$ values. The distinct trends are also observed between carbonate oversaturated waters and unsaturated waters in plot of river water $\delta^{26}\text{Mg}$ and suspended load $\delta^{26}\text{Mg}$ (Fig. 6). A negative

relationship for oversaturated waters also illustrates the formation of secondary carbonate which drifts the river water $\delta^{26}\text{Mg}$ higher and the suspended load $\delta^{26}\text{Mg}$ lower at the same time.

Rayleigh equation was constructed for Mg isotope fractionation process during carbonate precipitation:

$$\delta^{26}\text{Mg}_{\text{river}} = \delta^{26}\text{Mg}_{\text{origin}} + 1000(\alpha_{\text{calcite-solution}}^{\text{calcite}} - 1) \times \ln(1 - \gamma) \quad (3)$$

In the equation, γ refers to the fraction of Mg incorporated in carbonate. $\delta^{26}\text{Mg}_{\text{origin}}$ is $\delta^{26}\text{Mg}$ value of the origin solution where the secondary carbonate is formed and gains its Mg. An initial isotopic composition of -1.1‰ is employed for $\delta^{26}\text{Mg}_{\text{origin}}$, which is the $\delta^{26}\text{Mg}$ values of magnesium salt. The kinetic equilibrium precipitation of carbonate drives the river water $\delta^{26}\text{Mg}$ to -0.59‰ (the highest value of the oversaturated water). Then we can estimate that the fraction of Mg incorporated into secondary carbonate could be 16% for the given fractionation factor ($\alpha_{\text{calcite-solution}}$) between calcite and residue fluid of 0.997

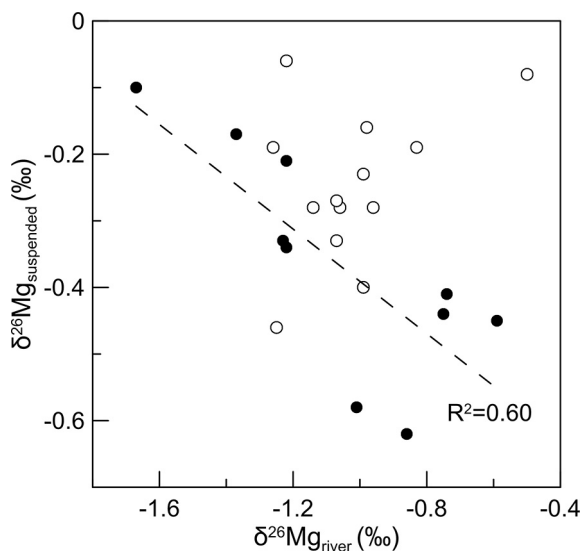


Fig. 6. Plot of $\delta^{26}\text{Mg}$ in river water versus $\delta^{26}\text{Mg}$ in suspended load.

(Mavromatis et al., 2013). Mg partition coefficient between calcite and fluid is as low as 0.01–0.03 (Mavromatis et al., 2013; Drake et al., 2018), the Ca precipitated would be 2–3 order of magnitudes more than Mg. As shown in Fig. 7, DSI show better correlation with $\delta^{26}\text{Mg}$ value of river waters relative to CSI. We infer that the secondary Mg-rich carbonate formation (such as high-Mg calcite, Whipkey et al., 2002, and pedogenic dolomite, Capo et al., 2000) might be an alternative mechanism incorporating Mg and fractionate Mg isotopes in the studied basin, since dolomite could form in any natural solution with Mg/Ca ratios as low as 1:1, as long as crystallization rate is slow enough for ordering to take place (Folk and Land, 1975).

Carbonate precipitations have been well documented previously, especially carbonate phases which are associated with calcium/magnesium-sulfate deposits (e.g.

Plummer et al., 1990). The dissolution of the sulfates (gypsum and epsomite) releases Ca and Mg to the pore fluids, promoting the carbonate precipitation processes. As calcite precipitates during evaporation, Ca^{2+} is rapidly depleted in the solutions. In absence of substantial recharge, continuous calcite precipitation (and the dissolution of Mg-evaporites) drives the solution Mg/Ca ratios higher, and resulted in Mg carbonate precipitation (Capo et al., 2000). Mg/Ca ratio in solution usually affects the Mg content in precipitated carbonate (Folk and Land, 1975). These ongoing processes have been reported in soil water and groundwater at basin scale (Capo et al., 2000; Whipkey et al., 2002; Trostle et al., 2014; Zhang et al., 2018), and regulate the river water geochemistry.

The influence of carbonate precipitation on Mg isotope signature of river waters at basin scale has aroused intense interests in previous studies (Tipper et al., 2006a; Brenot et al., 2008; Pogge von Strandmann et al., 2012; Lee et al., 2014; Fan et al., 2016). However, its effect on river Mg isotope composition has not been well recognized yet, because (1) calcite is not a significant sink for Mg, (2) the formation of high-Mg carbonate is difficult in most environment, and (3) Mg isotope fractionation signal could be obscured by repetitive dissolution/precipitation cycles (e.g. Brenot et al., 2008). In arid basins like upper-middle reaches of Jinsha River, we provide river geochemistry and Mg isotope evidence that carbonate precipitation is an important mechanism driving $\delta^{26}\text{Mg}$ of river waters heavier in basin scale, which suggests Mg isotope system as a potential tracer to constrain and explore continental and oceanic carbonate precipitation, as well as Mg cycling.

5.5. Implications

Even for the Mg isotope compositions of the carbonate unsaturated water samples, they cannot be fully explained by conservative mixing (Fig. 5a). Although the in-place river waters are unsaturated with respect to carbonate, carbonate kinetic precipitation reactions are widely documented in groundwater/soil pore water systems in the

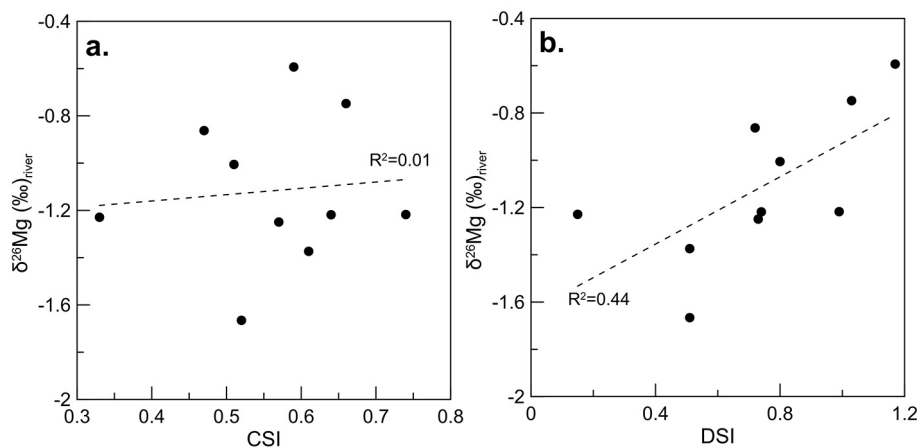


Fig. 7. Plots showing variations of $\delta^{26}\text{Mg}$ values with CSI (calcite saturation index) (a) and DSI (dolomite saturation index) in Jinsha River (b).

basin (Capo et al., 2000; Whipkey et al., 2002; Trostle et al., 2014; Zhang et al., 2018). Fractionation resulted solution (as a Mg reservoir) will be produced and serves as a new end-member, which recharges the river water and regulates river Mg isotope composition. The new end-member with heavy Mg isotope compositions will mix with rock weathering end-members to control the riverine $\delta^{26}\text{Mg}$. As shown in Fig. 5a, the carbonate unsaturated samples are distributed between silicate weathering end-member and those of oversaturated samples. This implies the mixing between the “carbonate precipitation produced Mg reservoir” and the silicate weathering Mg reservoir. Such fractionated reservoir is resulted from carbonate precipitation and the speculation could be well supported by the soil profile and groundwater studies, e.g. Trostle et al. (2014) speculated the export Mg flux from basalt soil is isotopically heavy (with $\delta^{26}\text{Mg}$ value of +3.2‰) due to the pedogenic carbonates in arid Hawaii Island. Authigenic soil high-Mg calcite and dolomite have also been reported in Hawaii soils (Capo et al., 2000; Whipkey et al., 2002). Recent work has also documented that the carbonate precipitation could elevate $\delta^{26}\text{Mg}$ value of groundwater by ~1‰ in north China (Zhang et al., 2018). This study proposes that the removal of light Mg during Mg carbonate precipitation can produce a fractionated reservoir for Mg at basin scale, and observably impact the riverine Mg isotope compositions and Mg cycling in arid-semiarid basins. Mg isotope composition of rivers transported to the oceans is controlled by the Mg isotope composition of the source lithology of upper continental crust and the fractionated reservoir (such as secondary minerals and plants) at global scale (Tipper et al., 2006a). Since the fractionation of Mg isotopes during carbonate precipitation is much larger than that of silicate secondary minerals (–2‰ to –3‰ vs. 0.01‰ to 0.6‰, Higgins and Schrag, 2010; Mavromatis et al., 2013; Ryu et al., 2016; Brewer et al., 2018), the influence of this fractionation reservoir should not be ignored. This process and further exploration on its effect during Mg cycling at different time and space scale are needed to be better constrained and considered.

6. CONCLUSIONS

The Mg isotopic composition of dissolved and suspended loads in Jinsha River falls into a range of 1.6‰. A lower $\delta^{26}\text{Mg}$ range of dissolved loads between –1.67‰ and –0.5‰ was observed, compared with suspended loads between –1.15‰ and –0.06‰. The atmospheric Mg precipitation and biologic impacts on riverine $\delta^{26}\text{Mg}$ values are negligible in Jinsha River Basin. Based on mass balance and mixing equations obtained from the river geochemistry data and related assumptions, lithological control and conservative mixing between different weathering end-members alone fails to fully explain Mg isotopic composition variations of Jinsha River waters. In evaporites and carbonates-dominated catchments, with limited silicate weathering contribution, the strong relationships between $\delta^{26}\text{Mg}$ and 1/Mg, and pH in carbonate oversaturated waters suggest secondary carbonate precipitation as the

principal process driving the Mg isotope composition heavier in Jinsha River Basin waters. In addition, the new Mg reservoir created by secondary carbonate formation acts as a new $\delta^{26}\text{Mg}$ end-member regulating river Mg isotope composition. The study proposes the secondary Mg carbonate resulted heavy Mg solution reservoir, and highlights its impact on river water Mg isotope composition at basin scale.

ACKNOWLEDGEMENTS

We thank Shan Ke for the assistance during Mg isotope analysis, and Minghui Li for providing samples. This work was financially supported by the “Strategic Priority Research Program” of the Chinese Academy of Sciences (Grant No. XDB26000000 and XDB15010405); the National Natural Science Foundation of China (Grant No. 91747202, 41730857 and 41402323).

APPENDIX A. SUPPLEMENTARY MATERIAL

Supplementary data to this article can be found online at <https://doi.org/10.1016/j.gca.2019.01.005>.

REFERENCES

- Black J. R., Epstein E., Rain W. D., Yin Q. Z. and Casey W. H. (2008) Magnesium isotope fractionation during plant growth. *Environ. Sci. Technol.* **70**, 4072–4079.
- Bolou-Bi E. B., Poszwa A., Leyval C. and Vigier N. (2010) Experimental determination of magnesium isotope fractionation during higher plant growth. *Geochim. Cosmochim. Acta* **74**, 2523–2537.
- Brenot A., Cloquet C., Vigier N., Carignan J. and France-Lanord C. (2008) Magnesium isotope systematics of the lithologically varied Moselle river basin France. *Geochim. Cosmochim. Acta* **72**, 5070–5089.
- Brewer A., Teng F. Z. and Dethier D. (2018) Magnesium isotope fractionation during granite weathering. *Chem. Geol.* **501**, 95–103.
- Buhl D., Immenhauser A., Smeulders G., Kabiri L. and Richter D. K. (2007) Time series $\delta^{26}\text{Mg}$ analysis in speleothem calcite: Kinetic versus equilibrium fractionation, comparison with other proxies and implications for palaeoclimate research. *Chem. Geol.* **244**, 715–729.
- Capo R. C., Whipkey C. E., Blachere J. R. and Chadwick O. A. (2000) Pedogenic origin of dolomite in a basaltic weathering profile, Kohala peninsula, Hawaii. *Geology* **28**, 271–274.
- Drake H., Mathurin F. A., Zack T., Schafer T., Roberts N. M., Whitehouse M., Karlsson A., Broman C. and Astrom M. E. (2018) Incorporation of metals into calcite in a deep anoxic granite aquifer. *Environ. Sci. Technol.* **52**, 493–502.
- Dürr H. H., Meybeck M. and Dürr S. H. (2005) Lithologic composition of the earth’s continental surfaces derived from a new digital map emphasizing riverine material transfer. *Global Biogeochem. Cycles* **19**, 49–53.
- Editorial Committee of Geology of Three River, Ministry of Geology and Mineral Resources. (1986) Geological Map of Nujiang, Lancang and Jinsha Rivers Area. Geological Publishing House.
- Elderfield H. and Schultz A. (1996) Mid-ocean ridge hydrothermal fluxes and the chemical composition of the ocean. *Annu. Rev. Earth Planet. Sci.* **24**, 191–224.

- Fan B., Zhao Z. Q., Tao F., Li X., Tao Z., Gao S. and He M. (2016) The geochemical behavior of Mg isotopes in the Huanghe basin China. *Chem. Geol.* **426**, 19–27.
- Folk R. L. and Land L. S. (1975) Mg/Ca ratio and salinity: Two controls over crystallization of dolomite. *Am. Assoc. Pet. Geol. Bull.* **59**, 60–68.
- Gaillardet J., Dupre B., Louvat P. and Allegre C. (1999) Global silicate weathering and CO₂ consumption rates deduced from the chemistry of large rivers. *Chem. Geol.* **159**, 3–30.
- Galy A. and France-Lanord C. (1999) Weathering processes in the Ganges-Brahmaputra Basin and the riverine alkalinity budget. *Chem. Geol.* **159**, 31–60.
- Galy A., Bar-Matthews M., Halicz L. and O’Nions R. K. (2002) Mg isotopic composition of carbonate: insight from speleothem formation. *Earth Planet. Sci. Lett.* **201**, 105–115.
- Geske A., Goldstein R. H., Mavromatis V., Richter D. K., Buhl D., Kluge T., John C. M. and Immenhauser A. (2015) The magnesium isotope ($\delta^{26}\text{Mg}$) signature of dolomites. *Geochim. Cosmochim. Acta* **149**, 131–151.
- Higgins J. A. and Schrag D. P. (2010) Constraining magnesium cycling in marine sediments using magnesium isotopes. *Geochim. Cosmochim. Acta* **74**, 5039–5053.
- Higgins J. A. and Schrag D. P. (2012) Records of Neogene seawater chemistry and diagenesis in deep-sea carbonate sediments and pore fluids. *Earth Planet. Sci. Lett.* **357–358**, 386–396.
- Higgins J. A. and Schrag D. P. (2015) The Mg isotopic composition of Cenozoic seawater-evidence for a link between Mg-clays, seawater Mg/Ca, and climate. *Earth Planet. Sci. Lett.* **416**, 73–81.
- Huang K. J., Teng F. Z., Wei G. J., Ma J. L. and Bao Z. Y. (2012) Adsorption- and desorption-controlled magnesium isotope fractionation during extreme weathering of basalt in Hainan Island China. *Earth Planet. Sci. Lett.* **359–360**, 73–83.
- Jacobson A. D., Blum J. D. and Walter L. M. (2002) Reconciling the elemental and Sr isotope composition of Himalayan weathering fluxes: insights from the carbonate geochemistry of stream waters. *Geochim. Cosmochim. Acta* **66**, 3417–3429.
- Jacobson A. D., Zhang Z., Lundstrom C. and Huang F. (2010) Behavior of Mg isotopes during dedolomitization in the Madison Aquifer South Dakota. *Earth Planet. Sci. Lett.* **297**, 446–452.
- Jiang H., Liu W. J., Xu X. F., Zhou X. D., Zheng Z. Y., Zhao T., Zhou L., Zhang X., Xu Y. F. and Liu T. Z. (2018) Chemical weathering of small catchments on the Southeastern Tibetan Plateau I: Water sources, solute sources and weathering rates. *Chem. Geol.* **500**, 159–174.
- Ke S., Teng F. Z., Li S. G., Gao T., Liu S. A., He Y. and Mo X. (2016) Mg, Sr, and O isotope geochemistry of syenites from northwest Xinjiang, China: Tracing carbonate recycling during Tethyan oceanic subduction. *Chem. Geol.* **437**, 109–119.
- Krishnaswami S. and Singh S. K. (1999) Silicate and carbonate weathering in the drainage of the Ganga-Ghaghara-Indus head waters: Contributions to major ion and Sr isotope geochemistry. *J. Earth Syst. Sci.* **107**, 283–291.
- Lee S. W., Ryu J. S. and Lee K. S. (2014) Magnesium isotope geochemistry in the Han River, South Korea. *Chem. Geol.* **364**, 9–19.
- Li W. Y., Teng F. Z., Ke S., Rudnick R. L., Gao S., Wu F. Y. and Chappell B. W. (2010) Heterogeneous magnesium isotopic composition of the upper continental crust. *Geochim. Cosmochim. Acta* **74**, 6867–6884.
- Liu S. A., Teng F. Z., He Y., Ke S. and Li S. (2010) Investigation of magnesium isotope fractionation during granite differentiation: implication for Mg isotopic composition of the continental crust. *Earth Planet. Sci. Lett.* **297**, 646–654.
- Mavromatis V., Gautier Q., Bosc O. and Schott J. (2013) Kinetics of Mg partition and Mg stable isotope fractionation during its incorporation in calcite. *Geochim. Cosmochim. Acta* **114**, 188–203.
- Moon S., Huh Y., Qin J. and van Pho N. (2007) Chemical weathering in the Hong (Red) River basin: Rates of silicate weathering and their controlling factors. *Geochim. Cosmochim. Acta* **71**, 1411–1430.
- Noh H., Huh Y., Qin J. and Ellis A. (2009) Chemical weathering in the Three Rivers region of Eastern Tibet. *Geochim. Cosmochim. Acta* **73**, 1857–1877.
- Opfergelt S., Georg R. B., Delvaux B., Cabidoche Y. M., Burton K. W. and Halliday A. N. (2012) Mechanisms of magnesium isotope fractionation in volcanic soil weathering sequences Guadeloupe. *Earth Planet. Sci. Lett.* **341–344**, 176–185.
- Parkhurst D. L. and Appelo C. A. J. (1999) User’s guide to PHREEQC - a computer program for speciation, batch-reaction, one-dimensional transport, and inverse geochemical calculations. U.S. Geol. Surv. Denver, Colorado.
- Plummer L. N., Busby J. F., Lee R. W. and Hanshaw B. B. (1990) Geochemical modeling of the madison aquifer in parts of Montana, Wyoming, and South Dakota. *Water Resour. Res.* **26**, 1981–2014.
- Pogge von Strandmann P. A. E., Burton K. W., James R. H., van Calsteren P., Gislason S. R. and Sigfússon B. (2008) The influence of weathering processes on riverine magnesium isotopes in a basaltic terrain. *Earth Planet. Sci. Lett.* **276**, 187–197.
- Pogge von Strandmann P. A. E., Opfergelt S., Lai Y. J., Sigfússon B., Gislason S. R. and Burton K. W. (2012) Lithium, magnesium and silicon isotope behavior accompanying weathering in a basaltic soil and pore water profile in Iceland. *Earth Planet. Sci. Lett.* **339**, 11–23.
- Pokrovsky B. G., Mavromatis V. and Pokrovsky O. S. (2011) Covariation of Mg and C isotopes in late Precambrian carbonates of the Siberian Platform: A new tool for tracing the change in weathering regime? *Chem. Geol.* **290**, 67–74.
- Qian H., Li M. Y., Ji Y. D., Yang B. C. and Zhao Z. H. (2007) Change of $\delta^{18}\text{O}$ and δD along the Dousitu River, Inner Mongolia, China, and their evidence of river water evaporation. *Aquat. Geochem.* **13**, 127–142.
- Ren F. P., Zhang P. C., Chen X. P., Xu P. and Chen J. (2016) Vegetation spatial heterogeneity of valleys along the Jinsha River and its influence on ecological restoration. *J. Yangtze Riv. Sci. Res. Inst.* **33**, 24–30.
- Riechelmann S., Buhl D., Schroder-Ritzrau A., Spötl C., Riechelmann D. F. C., Richter D. K., Kluge T., Marx T. and Immenhauser A. (2012) Hydrogeochemistry and fractionation pathways of Mg isotopes in a continental weathering system: Lessons from field experiments. *Chem. Geol.* **300**, 109–122.
- Ryu J. S., Vigier N., Decarreau A., Lee S. W., Lee K. S., Song H. and Petit S. (2016) Experimental investigation of Mg isotope fractionation during mineral dissolution and clay formation. *Chem. Geol.* **445**, 135–145.
- Telus M., Dauphas N., Moynier F., Tissot F. L. H., Teng F. Z., Nabelek P. I., Craddock P. R. and Groat L. A. (2012) Iron, zinc, magnesium and uranium isotopic fractionation during continental crust differentiation: The tale from migmatites, granitoids, and pegmatites. *Geochim. Cosmochim. Acta* **97**, 247–265.
- Teng F. Z., Wadhwa M. and Helz R. T. (2007) Investigation of magnesium isotope fractionation during basalt differentiation: Implications for a chondritic composition of the terrestrial mantle. *Earth Planet. Sci. Lett.* **261**, 84–92.
- Tian T. Y., Bao Y. R., Meng X. S., Wang S. and Chang X. (2017) Analysis of inorganic elements in gypsum fibrosum from

- different origins based on ICP-MS. *Chin. Arch. Tradit. Chin. Med.* **35**, 1041–1043.
- Tian H. C., Yang W., Li S. G., Ke S. and Duan X. Z. (2018) Low $\delta^{26}\text{Mg}$ volcanic rocks of Tengchong in Southwestern China: A deep carbon cycle induced by supercritical liquids. *Geochim. Cosmochim. Acta* **240**, 191–219.
- Tipper E. T., Galy A. and Bickle M. J. (2006a) Riverine evidence for a fractionated reservoir of Ca and Mg on the continents: Implications for the oceanic Ca cycle. *Earth Planet. Sci. Lett.* **247**, 267–279.
- Tipper E. T., Galy A., Gaillardet J., Bickle M. J., Elderfield H. and Carder E. A. (2006b) The magnesium isotope budget of the modern ocean: Constraints from riverine magnesium isotope ratios. *Earth Planet. Sci. Lett.* **250**, 241–253.
- Tipper E. T., Galy A. and Bickle M. J. (2008) Calcium and magnesium isotope systematics in rivers draining the Himalaya-Tibetan-Plateau region: Lithological or fractionation control? *Geochim. Cosmochim. Acta* **72**, 1057–1075.
- Tipper E. T., Gaillardet J., Louvat P., Capmas F. and White A. F. (2010) Mg isotope constraints on soil pore-fluid chemistry: Evidence from Santa Cruz California. *Geochim. Cosmochim. Acta* **74**, 3883–3896.
- Tipper E. T., Calmels D., Gaillardet J., Louvat P., Capmas F. and Dubacq B. (2012) Positive correlation between Li and Mg isotope ratios in the river waters of the Mackenzie Basin challenges the interpretation of apparent isotopic fractionation during weathering. *Earth Planet. Sci. Lett.* **333**, 35–45.
- Trostle K., Derry L., Vigier N. and Chadwick O. (2014) Magnesium isotope fractionation during arid pedogenesis on the Island of Hawaii (USA). *Proc. Earth Planet. Sci.* **10**, 243–248.
- Wang X., Metcalfe I., Jian P., He L. and Wang C. (2000) The Jinshajiang-Ailaoshan Suture Zone, China: tectonostratigraphy, age and evolution. *J. Asian Earth Sci.* **18**, 675–690.
- Whipkey C. E., Capo R. C., Hsieh J. C. C. and Chadwick O. A. (2002) Development of magnesian carbonate in Quaternary soils on the island of Hawaii. *J. Sediment. Res.* **72**, 158–165.
- Wimpenny J., Burton K. W., James R. H., Gannoun A., Mokadem F. and Gislason S. R. (2011) The behavior of magnesium and its isotopes during glacial weathering in an ancient shield terrain in West Greenland. *Earth Planet. Sci. Lett.* **304**, 260–269.
- Wimpenny J., Colla C. A., Yin Q. Z., Rustad J. R. and Casey W. H. (2014) Investigating the behavior of Mg isotopes during the formation of clay minerals. *Geochim. Cosmochim. Acta* **128**, 178–194.
- Wu W., Yang J., Xu S. and Yin H. (2008) Geochemistry of the headwaters of the Yangtze River, Tongtian He and Jinsha Jiang: Silicate weathering and CO_2 consumption. *Appl. Geochem.* **23**, 3712–3727.
- Yang Y., Fang X., Galy A., Zhang G., Liu S., Zan J., Wu F., Meng Q., Ye C., Yang R. and Liu X. (2015) Carbonate composition and its impact on fluvial geochemistry in the NE Tibetan Plateau region. *Chem. Geol.* **410**, 138–148.
- Yoon J., Huh Y., Lee I., Moon S., Hoh H. and Qin J. (2008) Weathering processes in the Min Jiang: major elements, $^{87}\text{Sr}/^{86}\text{Sr}$, $\delta^{34}\text{S}_{\text{SO}_4}$, and $\delta^{18}\text{O}_{\text{SO}_4}$. *Aquat. Geochem.* **14**, 147–170.
- Young E. D. and Galy A. (2004) The isotope Geochemistry and Cosmochemistry of Magnesium. *Rev. Mineral. Geochem.* **55**, 197–230.
- Zhang N. N., He Y. Q., Cao J. J., Ho K. F. and Shen Z. X. (2012) Long-term trends in chemical composition of precipitation at Lijiang, southeast Tibetan Plateau, southwestern China. *Atmos. Res.* **106**, 50–60.
- Zhang H., Jiang X. W., Wan L., Ke S., Liu S. A., Han G., Guo H. and Dong A. (2018) Fractionation of Mg isotopes by clay formation and calcite precipitation in groundwater with long residence times in a sandstone aquifer, Ordos Basin China. *Geochim. Cosmochim. Acta* **237**, 261–274.
- Zheng M. P. and Liu X. F. (2010) Hydrochemistry and minerals assemblages of salt lakes in the Qinghai-Tibet Plateau, China. *Acta Geol. Sin.* **11**, 1585–1600.

Associate editor: Andrew D. Jacobson